PHOTONICS Research

Silicon intensity Mach–Zehnder modulator for single lane 100 Gb/s applications

Miaofeng Li,[1,2,3] Lei Wang,[2,3] Xiang Li,[2,3] Xi Xiao,[2,3,*] and Shaohua Yu[1,2,3]

[1]Wuhan National Laboratory for Optoelectronics, School of Optical and Electronic Information, Huazhong University of Science and Technology, Wuhan 430074, Hubei, China
[2]State Key Laboratory of Optical Communication Technologies and Networks, Wuhan Research Institute of Posts & Telecommunications, Wuhan 430074, Hubei, China
[3]National Information Optoelectronics Innovation Center, Wuhan 430074, Hubei, China
*Corresponding author: xxiao@wri.com.cn

Received 27 October 2017; revised 10 December 2017; accepted 10 December 2017; posted 11 December 2017 (Doc. ID 309808); published 24 January 2018

In this paper, a substrate removing technique in a silicon Mach–Zehnder modulator (MZM) is proposed and demonstrated to improve modulation bandwidth. Based on the novel and optimized traveling wave electrodes, the electrode transmission loss is reduced, and the electro-optical group index and 50 Ω impedance matching are improved, simultaneously. A 2 mm long substrate removed silicon MZM with the measured and extrapolated 3 dB electro-optical bandwidth of >50 GHz and 60 GHz at the −8 V bias voltage is designed and fabricated. Open optical eye diagrams of up to 90 GBaud/s NRZ and 56 GBaud/s four-level pulse amplitude modulation (PAM-4) are experimentally obtained without additional optical or digital compensations. Based on this silicon MZM, the performance in a short-reach transmission system is further investigated. Single-lane 112 Gb/s and 128 Gb/s transmissions over different distances of 1 km, 2 km, and 10 km are experimentally achieved based on this high-speed silicon MZM.

OCIS codes: (250.7360) Waveguide modulators; (130.4110) Modulators; (130.3120) Integrated optics devices.

https://doi.org/10.1364/PRJ.6.000109

1. INTRODUCTION

Driven by the exponential growth of network traffic, bandwidth, energy consumption, and cost become the main obstacles to further increase channel capacity. Photonic integrated circuits (PICs) are regarded as the most promising way to overcome these bottlenecks [1]. Low cost integrated optical modulators are key components for future low-cost and energy-efficient PICs for optical transceivers [2]. To satisfy the everlasting demand of bandwidth, it is highly desirable that the modulators can work at high baud rates. Recently, the IEEE task force has discussed a 400 gigabit Ethernet (400 GbE) standard [3] to meet the fast-increasing bandwidth demands of short-reach optical interconnects for data centers, high-performance computers, etc. The 4 × 100 Gb/s schemes are becoming the preferable solutions to realize 400 Gb/s short-reach transmission, as a fewer number of lanes will benefit from smaller packaging size and lower power consumption [4,5]. Therefore, the ultrahigh-speed electro-optical modulation techniques for single-lane 100 Gb/s modulation are essential for realizing a feasible 400 GbE optical transceiver.

Many efforts have been made to develop ultrahigh-speed optical modulators or direct modulated lasers for 100 Gb/s four-level pulse amplitude modulation (PAM-4). For example, a 60 GBaud/s PAM-4 eye-diagram has been demonstrated based on a plasmonic modulator [6]. A single line rate of up to 120 Gb/s PAM-4 modulation using a 0.5 mm long silicon organic hybrid Mach–Zehnder modulator (MZM) is realized in [7]. A single channel of 112 Gb/s PAM-4 transmission without pre-emphasis based on a short direct modulated laser is also achieved [8].

The silicon PIC is an ideal technology for reducing both the size and power consumption of a multilane optical transmitter, because multichannel modulators can be integrated in a single silicon chip [9] and co-packaged with CMOS driver circuits [10]. High-speed OOK signal transmissions at 56 Gb/s based on the silicon modulators are recently demonstrated [10–15]. However, the bandwidths are normally limited to 30 ∼ 40 GHz, making it difficult to further increase the serial data rate to 100 Gb/s without high cost and power consumption electrical chips for bandwidth equalization. To further reduce the component bandwidth requirement, a PAM-4 format is used to increase the spectral efficiency; 112 Gb/s and 128 Gb/s PAM-4 transmissions using SiP MZM are demonstrated [16,17], while the DACs are used to pre-compensate the limited modulation bandwidth. Therefore, a silicon modulator with ultrahigh bandwidth for high symbol rate OOK and

PAM-4 signal generation without using complex and high cost pre-equalization circuit is in great demand for 400 GbE transceivers.

The silicon electro-optical modulator based on the relatively weak carrier-depletion effect often has a long phase-shifting regions to reduce the driving voltages [18]. It requires traveling wave electrode designs rather than the lumped ones. For a high-speed traveling wave Mach–Zehnder modulator (TWMZM), three core aspects need to be carefully designed [19]: the microwave attenuation, the velocity mismatch between the microwave and optical wave, and the impedance matching of the traveling wave electrode. The bandwidth of a silicon TWMZM is mainly determined by the microwave loss of the whole modulator when the velocity and the impedance match at the same time. To increase the bandwidth of the modulator, significant efforts have been made to reduce the microwave loss. By optimizing the series resistance [20] of the active region and using the single-drive series push-pull PN junction structures [21], the microwave loss of the PN junction is reduced to a large extent. Other methods such as using Cu electrodes and Ti/TiN/AlCu electrodes are also investigated to minimize the electrodes' microwave skin loss [22,23]. Currently, most works are mainly focusing on reducing the PN junction and electrode loss. However, little work has been done to reduce the substrate silicon caused loss.

In this work, we present the design and realization of a high-speed SiP MZM for single channel of 100 Gb/s optical transmissions. The substrate removing technique is introduced for the bandwidth improvement, which reduces the electrode transmission loss, improves the electro-optical group index matching, and achieves 50 Ω impedance matching, simultaneously. The measured and extrapolated 3 dB electro-optical bandwidth of beyond 50 GHz is achieved, and the highest OOK signal transmission at 90 GBaud/s is experimentally demonstrated. The DAC-less PAM-4 modulation up to 56 GBaud/s is also experimentally demonstrated. At last, successful transmission experiments of single-lane 112 Gb/s and 128 Gb/s PAM-4 over 1, 2, and 10 km based on this modulator are demonstrated.

2. DEVICE DESIGN AND FABRICATION

A general structure of the substrate removed SiP MZM is depicted in Fig. 1. The device is fabricated on a high-resistance silicon-on-insulator (SOI) wafer with a 220 nm thick silicon layer and a 3 μm thick buried oxide (BOX). The MZM comprised two 2 mm long active waveguides and ground-signal electrode. The electrode has a width of 30 μm and a gap of 16 μm, which is fabricated in the top 2 μm thick aluminum metal layer defined as metal2. Another metal layer below the metal2 is defined as metal1, which is used to facilitate the electrical connections. The rib waveguides are 550 nm wide with a slab thickness of 90 nm. A lateral PN junction is embedded into each arm with a junction interface offset of 50 nm from the waveguide center to the N type region. The doping concentration of the PN junction is nonuniform in the vertical direction, which varies from 0.8×10^{18} cm^{-3} to 1.5×10^{18} cm^{-3}. Intermediate P+ and N+ doping regions of doping concentrations of 2×10^{18} cm^{-3} are added 200 nm away from the PN junction. The intermediate doping region is used to further reduce the series resistance R_{pn} of the PN junction while keeping a low optical loss. The P++ and N++ regions with a concentration of 1×10^{20} cm^{-3} are 1000 nm away from the PN junction for ohmic contact. The two PN junctions are connected in series to form a push–pull configuration, which helps to reduce the capacitance and improve the impedance matching [21,24]. The single-drive push-pull structure will double the driving voltage compared with the dual-drive configuration. A DC bias voltage is applied to the connected N++ region to deplete the carriers in the PN junctions during the modulation process. An on-chip terminator with a 35 Ω resistance is connected to the end of the RF electrode. Two 1 × 2 multimode interferences are used to form the Mach–Zehnder interferometer. A power-efficient phase shifter is integrated on one active arm to tune the bias condition of the MZM. The phase shifter is formed by a doped silicon resistor. The tuning power is 1 ∼ 2 mW for a π phase shift, which is realized by etching the thermal insulation trenches around the silicon slabs. The substrate removing process is the same as that of fabrication of the suspended heater. The patterns of the deep trenches are first patterned beside the electrodes. Then, a SiO_2 dry etching process is followed to etch the trenches down to the silicon substrate. Finally, an isotropic silicon dry etching is performed to remove the silicon under the electrode.

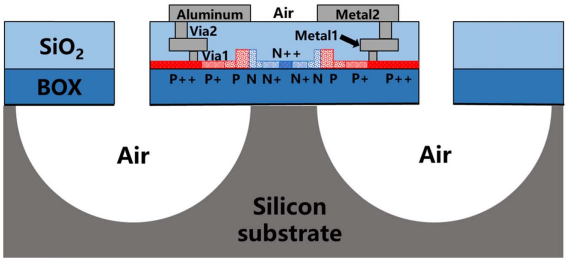

Fig. 1. Diagram of the cross-sectional structure.

To explain the basic principle of the substrate removing technique, we first analyze the bandwidth limitation factors of a depletion-type silicon TWMZM. During the dynamic signal modulation process, three paths of current flow pass from the signal electrode to the ground [25]: the current through the PN junction, through the electrode and the substrate. All three current paths will cause the frequency dependent power consumption, which results in bandwidth degradation of the silicon TWMZM. The power consumption of the junction is useful for signal modulation and can be minimized by reducing the PN junction series resistance or by using the series PN junction structures. However, the power consumed by the electrode and substrate is useless and will lead to a decline of bandwidth. In order to reduce the loss of the electrode, a lot of efforts have been made by using Cu electrodes, Ti/TiN/AlCu electrodes, and so on. Currently, few studies have focused on the loss of the substrate to improve the bandwidth. However, we find that the silicon substrate has a significant impact on the microwave mode and loss.

The mode field distributions before and after the silicon substrate is removed are shown in Fig. 2. The distributions

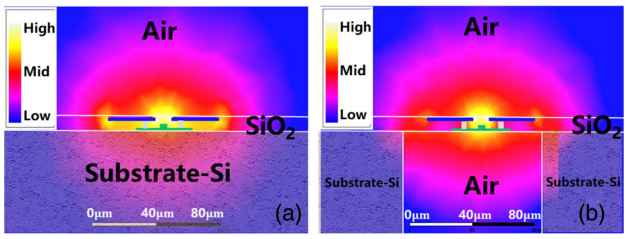

Fig. 2. Microwave electrical mode distribution of the TWMZM cross section (a) before and (b) after the silicon substrate is removed.

are obtained from a 3D full-wave electromagnetic software based on the finite element method (FEM) simulation. For the conventional electrode structure with the silicon substrate, a large proportion of the electric field mode is distributed in the silicon substrate, as shown in Fig. 2(a). The electrical mode field distribution pattern is pulling down to the high permittivity silicon substrate region, which will cause the diffusion of the mode and a higher refractive index. At the same time, the electrical mode has a large overlap with the silicon substrate, which will cause a higher microwave transmission loss. If we take measures to etch away the silicon substrate under the electrode, mode distribution will be confined. Through the simulations, the mode field distribution of the substrate removed modulator cross-section is shown in Fig. 2(b). We can find that the mode overlaps with the silicon substrate, and the highly doped slabs are reduced to a large extent.

To illustrate the key difference in microwave loss between the conventional electrode structure and the substrate removed electrode, we analyze the RF electrode design used in our work with co-planar strip (CPS) transmission lines. To more clearly illustrate the loss improvement of the substrate removing technique, the PN junction is not included in all the simulations in this part. It indicates that the silicon substrate has a direct and obvious impact on the modulator bandwidth. Very high silicon substrate resistance such as 1000 $\Omega \cdot$ cm would ensure lower loss and higher bandwidth. However, we can further reduce the loss by 1 dB/cm after directly removing the 1000 $\Omega \cdot$ cm high-resistance silicon substrate, as depicted in the simulation results in Fig. 3.

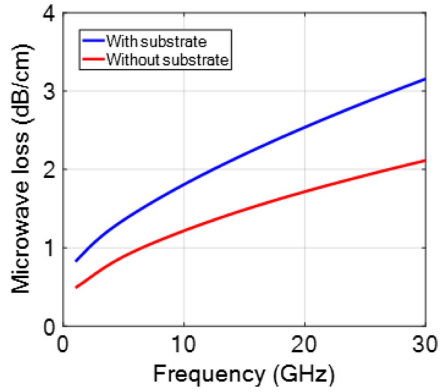

Fig. 3. Microwave attenuation based on finite element method (FEM) simulations on unloaded CPS transmission lines before and after substrate removing of the wafer used in our design.

To further analyze the performance of the modulator before and after removing the silicon substrate, we numerically analyze the electro-optic bandwidth for both cases. The electro-optic bandwidth EO_{S21} of an optical modulator can be expressed as

$$\mathrm{EO}_{S21} = 10 \log \frac{|S21|^2 - 2 \cdot |S21| \cdot \cos(\beta_{\mathrm{opt}}^{\mu} \cdot l) + 1}{(\ln |S21|)^2 + (\beta_{\mathrm{opt}}^{\mu} \cdot l)^2}, \quad (1)$$

$$\beta_{\mathrm{opt}}^{\mu} = \frac{\omega_m}{c}(n_\mu - n_{\mathrm{opt}}), \quad (2)$$

where $S21$ is the electric forward transmission coefficient of the modulator scattering matrix; $\beta_{\mathrm{opt}}^{\mu}$ is defined in Eq. (2), which characterizes the velocity mismatch of the modulator; l is the traveling-wave electrode length of the modulator; ω_m is the modulation angular frequency; c is the velocity of light in vacuum; n_μ is the microwave refractive index and n_{opt} is the optical refractive index [26].

By combining the simulated electrical loss, RF impedance, and EO effective index, the EO bandwidth is calculated and shown in Fig. 4. The simulated EO responses of the TWMZM before and after removing the silicon substrate are both plotted in Fig. 4. The 3 dB EO bandwidth is 55 GHz at 5 V reverse bias after removing the silicon substrate. It should be noted that the 3 dB EO bandwidth is only 47 GHz when the substrate is not removed. Therefore, the 3 dB EO bandwidth is increased by 17% with our proposed technique, which sufficiently proves the validity of this technique.

Based on the above design, the silicon substrate removed modulator is fabricated. In the edge coupler and suspended heater fabrication process, a more than 100 μm deep Si trench is etched. It should be noted that the substrate removing process for the modulator is the same as the fabrications of the suspended heater and the edge coupler. The substrate removing technique does not increase the complexity of the process flow. That means we use the same substrate removing process to improve the EO bandwidth, the thermal phase shifter efficiency, and the optical edge coupler loss. The fabrication steps are shown in Fig. 5. An optimum length of 2 mm is chosen for the trade-off between extinction ratio and bandwidth. Both types of modulator with and without the silicon substrate are fabricated to evaluate the effect of the substrate removing technique. Figure 6 shows the microscope photo of the substrate removed modulator after the whole fabrication processes.

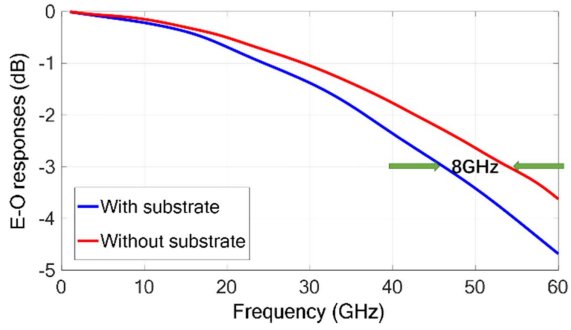

Fig. 4. Simulated EO $S21$ before and after substrate removal of the wafer used in our design.

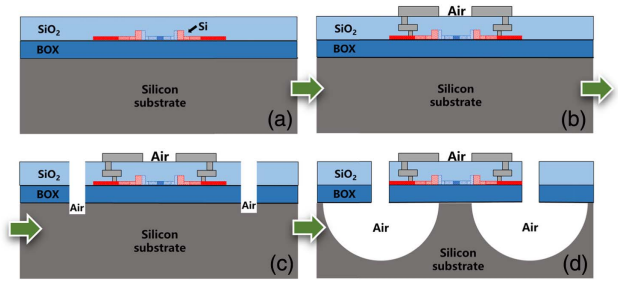

Fig. 5. Fabrication process of the substrate removed modulator based on IME's silicon photonics platform.

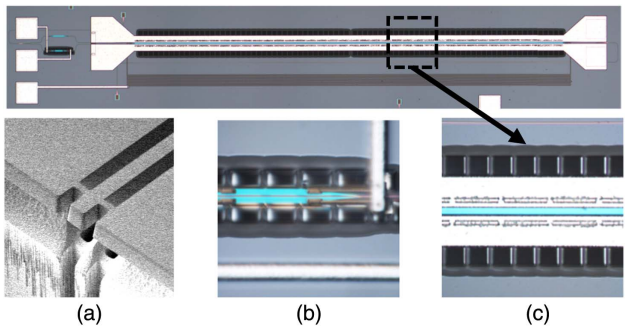

Fig. 6. Micrograph of the fabricated substrate removed silicon modulator viewed from above and the enlarged picture of the (a) edge couple, (b) phase shifter, and (c) the electrode region.

3. DEVICE CHARACTERIZATION

The DC V_π of the fabricated 2 mm long modulator is 7 V under −4 V bias, corresponding to a modulation efficiency figure-of-merit of 1.4 V·cm. The insertion loss is measured to be 5.4 dB, which includes 0.6 dB waveguide loss, 4.4 dB phase shifter loss, and 0.4 dB from the two MMIs. Two 50 GHz GS high-frequency RF probes are used to test the modulator. The small signal properties are characterized by a 50 GHz Rohde & Schwarz vector network analyzer (VNA) at different DC bias voltages. Two grating couplers are used to couple light on and off the chip to simplify the testing process. The measured small signal properties of the substrate removed modulator at various DC bias voltages are presented in Fig. 7. The curves are normalized to the response at a reference frequency of 1 GHz. The measured electrical-electrical (EE) $S21$ at different reverse bias voltages are shown in Fig. 7(a). The −6.4 dB point is beyond 50 GHz at the reverse bias voltage of 6 V. The $S11$ parameter is less than −15 dB from DC to 40 GHz and less than −12 dB at all frequencies, indicating that the electrode impedance matches well with the 50 Ω source.

Removing the substrate silicon has several advantages. First, the air trenches reduce the refractive index of the electrical driving signal. Figure 7(b) compares the refractive index of the electrodes with and without silicon substrate, which are abstracted from the tested electrical $S21$ parameters at the DC bias voltage of 4 V. The refractive index is reduced by 0.3 – 0.4 and achieves a better matching to the optical waveguide's group index of 3.7 – 3.8. Second, the substrate removing technique raises the characteristic impedance of the modulator by reducing the capacitance of the electrode. Figure 7(c) shows the characteristic impedance of the electrodes with and without silicon substrate, which are calculated from the tested electrical $S21$

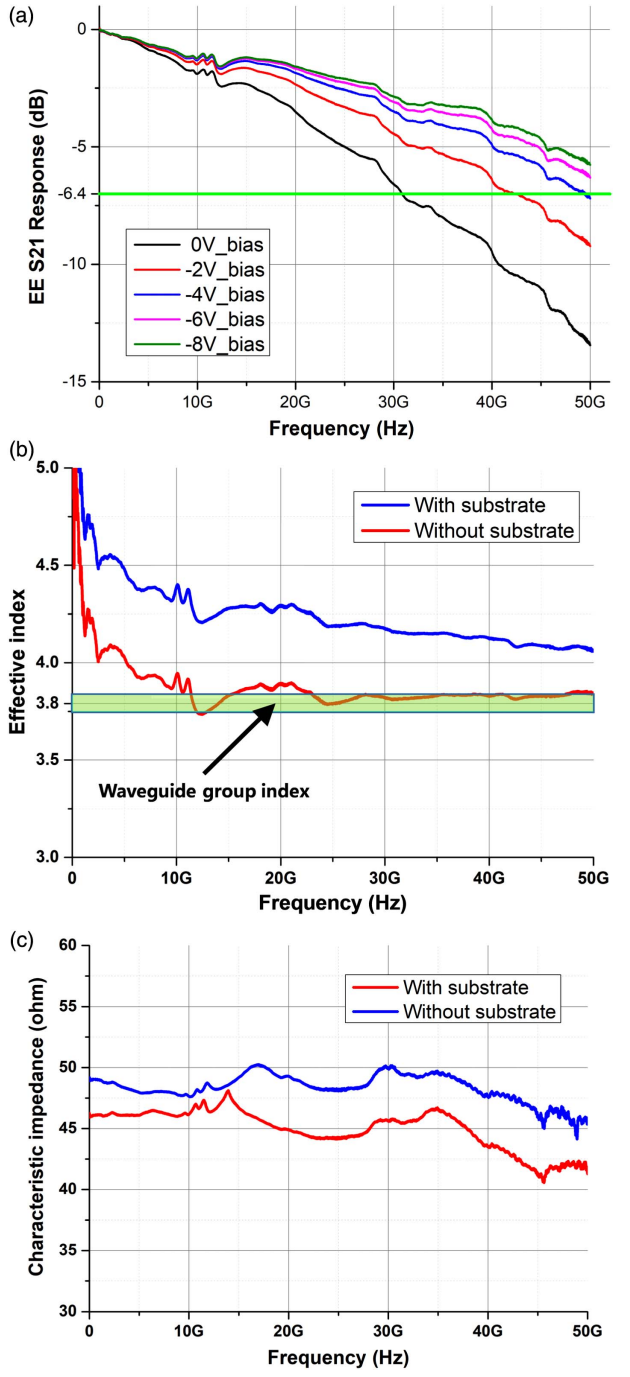

Fig. 7. (a) Measured EE $S21$ of the substrate removed modulator under various bias voltages. (b) Microwave index of the modulator before and after the silicon substrate is removed, which is extracted from the tested EE $S21$ at −4 V bias voltage. (c) Electrode characteristic impedance of the modulator before and after the silicon substrate is removed, which is calculated from the tested EE $S21$ and $S11$ at −4 V bias voltage.

and $S11$ parameters at the DC bias voltage of −4 V. The characteristic impedance rises by nearly 4 Ω, which helps to reduce the reflections of the driving signal. The tested results indicate that the refractive index is higher than the simulation results, and the impedance is lower than the simulation results, too. This is because the actual capacitance is higher than the calculated value in the simulation. The higher capacitance may be due to the fact that substrate in the fabricated substrate removed modulator is not completely removed, but the substrate in the simulation is completely removed.

Moreover, the air trench strengthens the electrode's field confinement and reduces the electrical propagation loss caused by the silicon substrate. We then characterize the small signal EO bandwidth of the device through S-parameter measurements using the same VNA and a 50 GHz EO bandwidth photodetector (PD). The EO bandwidth of the substrate removed modulator is then obtained by deducting the known EO S21 of the U2t PD. Figure 8 shows the measured EO $S21$ frequency responses at various bias voltages. The modulation response decays to 1.2 dB at 50 GHz compared with the DC state at DC bias voltage of −4 V, and the 3 dB bandwidth is predicted to be 58 GHz. The 3 dB EO bandwidth reaches 60 GHz at the DC bias voltage of −8 V, which is the highest bandwidth of a pure silicon MZM to the best of our knowledge. The 3 dB EO bandwidth is higher than the corresponding EE $S21$ at −6.4 dB point because we use a load of lower than 50 Ω to achieve the bandwidth peaking effect [25]. Bandwidth increases at the expense of increased power consumption in this situation.

Next, we test the large signal performance of the modulator using a Tektronix wideband oscilloscope. We first apply OOK optical modulations to test the modulator performance. The 64 G SHF 12104A pulse pattern generator (PPG) and an SHF 603A 2:1 multiplexer (MUX) are used to generate the electrical signals up to 90 GBaud/s. A 50 GHz broadband amplifier with output V_{pp} of 5 V is used to drive the modulator through a 40 GHz GGB GS microwave probe. The experimental setup is shown in Fig. 9. The optical eye diagrams without any pre-emphasis at 70, 80, and 90 GBaud/s are shown in Fig. 10. For

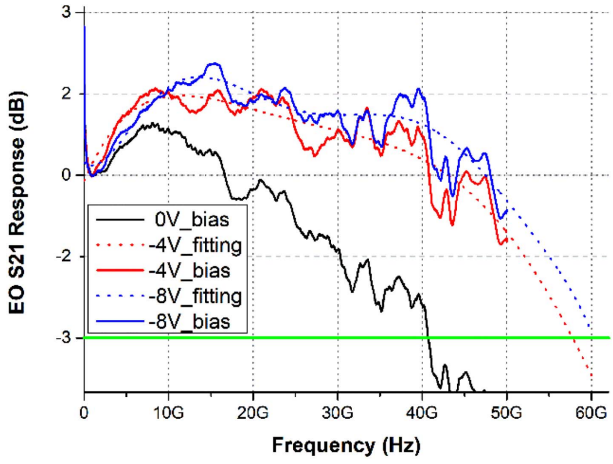

Fig. 8. Measured EO $S21$ response under various bias voltages after the silicon substrate is removed.

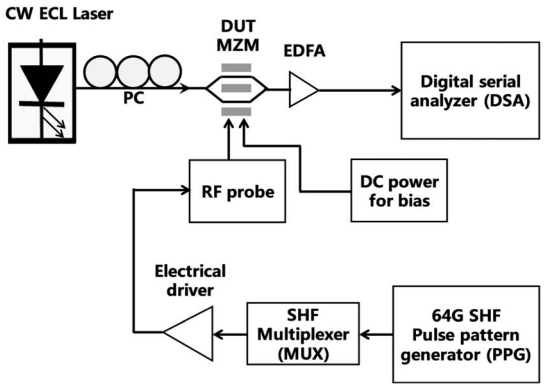

Fig. 9. Experimental setup for the substrate removed TWMZM OOK eye-diagram measurements.

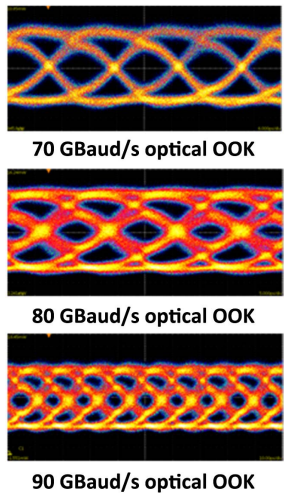

Fig. 10. Optical eye diagrams at the different rates of 70 GBaud/s, 80 GBaud/s, and 90 GBaud/s under the driving voltage of 5 V V_{pp} without any pre-emphasis under bias voltage of −6 V. The extinction ratios are 3.6 dB, 2.7 dB, and 3.3 dB, respectively.

all the measurements, the modulator is set at the quadrature point through the phase shifter. The modulation speed can be potentially improved to beyond 100 Gb/s by employing pre- or post-compensations on the electrical domain [27].

DAC-less PAM-4 experiments are also carried out to increase the modulation data rate. The experimental setup is depicted in Fig. 11. The output of PPG is two independent data with the identical V_{pp} of 500 mV. The electrical signal from one channel is attenuated by 6 dB and then combined with the other to form an electrical PAM-4 signal, which is then amplified by a linear driver SHF S807. The driving signal is also fed into the TWMZM by the 40 GHz GGB GS probe. The optical PAM-4 eye-diagrams at 28 GBaud/s, 50 GBaud/s, and 56 GBaud/s are shown in Fig. 12. The optical eye-diagram is clearly opened up to 56 GBaud/s. Due to the limited bandwidth of the probe and RF cables, the optical PAM-4 baud rate is limited to 56 GBaud/s. However, to the best of our knowledge, it is the highest PAM-4 modulation baud rate without

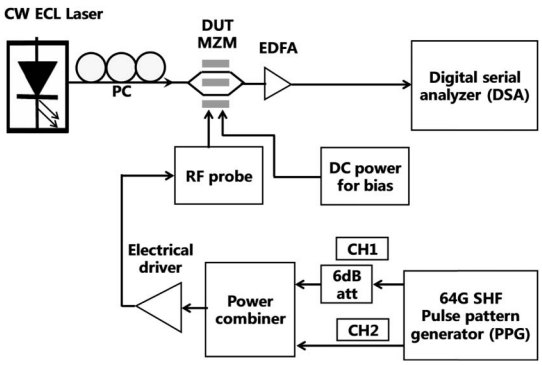

Fig. 11. Experimental setup for the substrate removed TWMZM PAM-4 eye-diagram measurements.

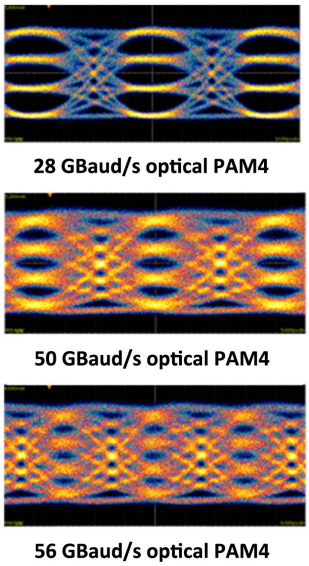

Fig. 12. Measured PAM-4 modulation optical eye diagrams at 28 GBaud/s, 50 GBaud/s, and 56 GBaud/s without any pre-emphasis under bias voltage of −6 V. The extinction ratios are 3.6 dB, 2.5 dB, and 2.7 dB, respectively.

any electrical compensations of pure silicon modulator, which demonstrates the effectiveness of the substrate removing technique.

4. TRANSMISSION EXPERIMENTS

In this section, we investigate the performance of the MZM for PAM-4 transmission. The experimental setup for the PAM-4 signal transmission using designed device under test (DUT) silicon photonics MZM is shown in Fig. 13. An external cavity laser (ECL) is used as the optical source. The wavelength of ECL is around 1550 nm, and the output power is set to 15 dBm. The PAM-4 signal is generated from an arbitrary waveform generator (AWG, M9502A) before being amplified by a linear driver (SHF, S804 A). The final swing voltage that drives the MZM is 3.8 V. Performances of both 56 GBaud/s and 64 GBaud/s PAM-4 signal transmissions are investigated.

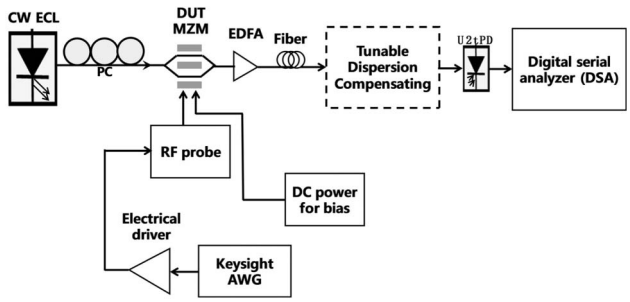

Fig. 13. Experimental setup for the PAM-4 signal transmission based on the substrate removed silicon modulator even different distances.

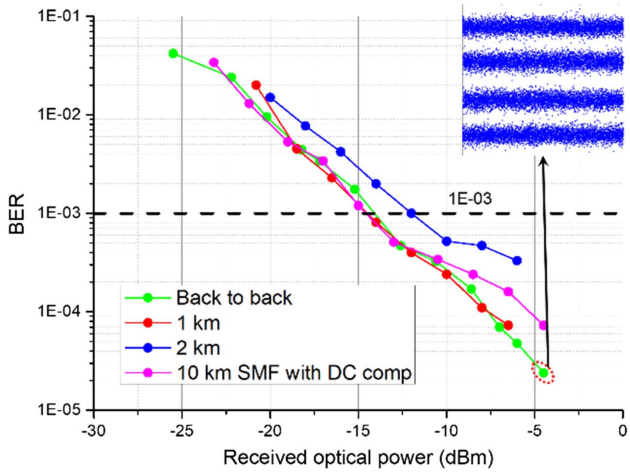

Fig. 14. Measured curve of BER versus the received optical power for 56 GBaud/s (112 Gb/s) PAM-4 signal transmission under bias voltage of −6 V.

The on-chip insertion loss of the silicon photonics MZM is 5.4 dB. A DC bias voltage is applied to the phase shifter to make sure the MZM works in the linear modulation region. An EDFA is used before the modulated signal launching into the single mode fiber (SMF) to adjust the launch power. In the receiver end, the received signal is first amplified by an EDFA. Then, the signal is detected by an U2t-PD with bandwidth of 50 GHz. The detected signal is sampled by an oscilloscope working at 160 GSa/s. The off-line DSP includes resampling at 2 SPS, matched filter, equalization, and symbol decision.

Figure 14 shows the measured curve of BER versus the received optical power (ROP) for 56 GBaud/s (112 Gb/s) PAM-4 signal transmission. In the measurements, a variable optical attenuator (VOA) is used to adjust the received optical power. Performances under different span lengths are investigated, including 1 km, 2 km, and 10 km SMF. It should be noted that a dispersion compensation module (DCM) is used in the 10 km case, where the CD is well compensated. A 1×10^{-3} FEC threshold is assumed for error-free transmission. The minimum achievable ROP for 56 GBaud/s PAM-4 is around −15 dBm for both optical back-to-back and 1 km transmission. A 2 km transmission introduces around 2 dB

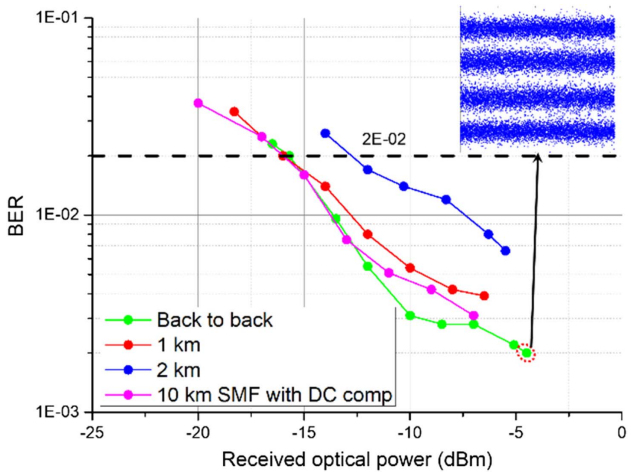

Fig. 15. Measured curve of BER versus the received optical power for 64 GBaud/s (128 Gb/s) PAM-4 signal transmission under bias voltage of −6 V.

penalty for the receiver sensitivity, which is mainly due to the CD. For the 10 km transmission with DCM, a similar result is observed as the optical back-to-back measurement. The corresponding restored PAM-4 signal is shown in Fig. 14.

Figure 15 shows the measured curve of BER versus the received optical power (ROP) for 64 GBaud/s (128 Gb/s) PAM-4 signal transmission. The minimum achievable ROP for 64 GBaud/s PAM-4 is around −16 dBm for both optical back-to-back and 1 km transmission, assuming the FEC threshold of 2×10^{-2}. A 2 km transmission introduces around 3 dB penalty for the receiver sensitivity, which is mainly due to the CD. For the 10 km transmission with DCM, a similar result is observed as the optical back-to-back measurement. The restored PAM-4 signal is also shown in the inset of Fig. 15.

5. CONCLUSION

The design and analysis of a silicon modulator with the silicon substrate removing technique for high EO bandwidth and impedance matching is presented for the first time. At a reverse bias voltage of 4 V, the measured EO modulation response shows a 1.2 dB drop at 50 GHz, and a 3 dB bandwidth of 58 GHz is achieved. The 3 dB EO bandwidth reaches 60 GHz at the DC bias voltage of −8 V, which, to the best of our knowledge, is the highest bandwidth of a pure silicon MZM. By applying this technique, the EO bandwidth of the same modulator has been increased by 8 GHz. At the same time, the reflection magnitude EE S11 remains below −10 dB over 50 GHz. A recorded high OOK serial modulation speed of 90 Gb/s is experimentally demonstrated. We also show DAC-free PAM-4 modulations from 28 to 56 GBaud/s based on this modulator; 112 Gb/s and 128 Gb/s PAM-4 signal over 10 km SMF transmission is experimentally demonstrated. The substrate removing technique proposed in this paper indicates that it is possible to create high bandwidth modulators in the silicon photonic technology. It is believed that our device has great potential to achieve low-cost and low-complexity 100 Gb/s modulation per lane for future 400 GbE transceiver.

REFERENCES

1. R. W. Tkach, "Scaling optical communications for the next decade and beyond," Bell Labs Tech. J. **14**, 3–9 (2010).
2. G. T. Reed, G. Mashanovich, F. Y. Gardes, and D. J. Thomson, "Silicon optical modulators," Nat. Photonics **4**, 518–526 (2010).
3. IEEE, "200 Gb/s and 400 Gb/s ethernet task force," IEEE P802.3bs, 2016, available at http://www.ieee802.org/3/bs/.
4. S. Kanazawa, T. Fujisawa, K. Takahata, H. Sanjoh, R. Iga, Y. Ueda, W. Kobayashi, and H. Ishii, "400-Gb/s operation of flip-chip interconnection EADFB laser array module," in *Optical Fiber Communications Conference* (2015), paper Tu3I.1.
5. P. Groumas, V. Katopodis, J. H. Choi, H.-G. Bach, J.-Y. Dupuy, A. Konczykowska, Z. Zhang, P. Harati, E. Miller, A. Beretta, L. Gounaridis, F. Jorge, V. Nodjiadjim, A. Dede, A. Vannucci, G. Cangini, R. Dinu, N. Keil, N. Grote, H. Avramopoulos, and C. Kouloumentas, "Multi-100 GbE and 400 GbE interfaces for intra-data center networks based on arrayed transceivers with serial 100 Gb/s operation," J. Lightwave Technol. **33**, 943–954 (2015).
6. C. Hoessbacher, A. Josten, B. Baeuerle, Y. Fedoryshyn, H. Hettrich, Y. Salamin, W. Heni, C. Haffner, C. Kaiser, R. Schmid, D. L. Elder, D. Hillerkuss, M. Möller, L. R. Dalton, and J. Leuthold, "Plasmonic modulator with >170 GHz bandwidth demonstrated at 100 GBd NRZ," Opt. Express **25**, 1762–1768 (2017).
7. H. Zwickel, S. Wolf, C. Kieninger, Y. Ku-Tuvantavida, M. Lauermann, T. De keulenaer, A. Vyncke, R. Vaernewyck, J. Luo, A. K.-Y. Jen, W. Freude, J. Bauwelinck, S. Randel, and C. Koos, "Silicon-organic hybrid (SOH) modulators for intensity-modulation/direct-detection links with line rates of up to 120 Gbit/s," Opt. Express **25**, 23784–23799 (2017).
8. Y. Matsui, T. Pham, W. A. Ling, R. Schatz, G. Carey, H. Daghighian, T. Sudo, and C. Roxlo, "55-GHz bandwidth short-cavity distributed reflector laser and its application to 112-Gb/s PAM-4," in *Optical Fiber Communications Conference* (2016), paper Th5B.4.
9. M. Streshinsky, A. Novack, R. Ding, Y. Liu, A. E.-J. Lim, P. G.-Q. Lo, T. Baehr-Jones, and M. Hochberg, "Silicon parallel single mode 48 × 50 Gb/s modulator and photodetector array," J. Lightwave Technol. **32**, 4370–4377 (2014).
10. G. Denoyer, A. Chen, B. Park, Y. Zhou, A. Santipo, and R. Russo, "Hybrid silicon photonic circuits and transceiver for 56 Gb/s NRZ 2.2 km transmission over single mode fiber," in *40th European Conference Optical Communication (ECOC)*, Cannes, France, September 2014, paper PD.2.4.
11. D. Patel, S. Ghosh, M. Chagnon, A. Samani, V. Veerasubramanian, M. Osman, and D. V. Plant, "Design, analysis, and transmission system performance of a 41 GHz silicon photonic modulator," Opt. Express **23**, 14263–14287 (2015).
12. X. Xiao, H. Xu, X. Y. Li, Z. Y. Li, T. Chu, Y. D. Yu, and J. Z. Yu, "High-speed, low-loss silicon Mach-Zehnder modulators with doping optimization," Opt. Express **21**, 4116–4125 (2013).
13. L. Chrostowski and M. Hochberg, *Silicon Photonics Design: From Devices to Systems* (Cambridge University, 2015).
14. R. Ding, Y. Liu, Y. Ma, Y. Yang, Q. Li, A. E.-J. Lim, G.-Q. Lo, K. Bergman, T. Baehr-Jones, and M. Hochberg, "High-speed silicon modulator with slow-wave electrodes and fully independent differential drive," J. Lightwave Technol. **32**, 2240–2247 (2014).
15. P. Dong, X. Liu, S. Chandrasekhar, L. L. Buhl, R. Aroca, and Y.-K. Chen, "Monolithic silicon photonic integrated circuits for compact 100+ Gb/s coherent optical receivers and transmitters," IEEE J. Sel. Top. Quantum Electron. **20**, 150–157 (2014).
16. M. Chagnon, M. Osman, M. Poulin, C. Latrasse, J.-F. Gagné, Y. Painchaud, C. Paquet, S. Lessard, and D. V. Plant, "Experimental study of 112 Gb/s short reach transmission employing PAM formats and SiP intensity modulator at 1.3 μm," Opt. Express **22**, 21018–21036 (2014).
17. A. Samani, D. Patel, M. Chagnon, E. Elfiky, R. Li, M. Jacques, N. Abadia, V. Veerasubramanian, and D. V. Plant, "Experimental parametric study of 128 Gb/s PAM-4 transmission system using a multi-electrode silicon photonic Mach Zehnder modulator," Opt. Express **25**, 13252–13262 (2017).
18. A. R. Soref and B. R. Bennett, "Electro optical effects in silicon," IEEE J. Quantum Electron. **23**, 123–129 (1987).

19. R. G. Walker, "High-speed III-V semiconductor intensity modulators," IEEE J. Quantum Electron. **27**, 654–667 (1991).
20. K. Ogawa, K. Goi, Y. T. Tan, T.-Y. Liow, X. Tu, Q. Fang, G.-Q. Lo, and D.-L. Kwong, "Silicon Mach-Zehnder modulator of extinction ratio beyond 10 dB at 10.0–12.5 Gbps," Opt. Express **20**, 6163–6169 (2012).
21. P. Dong, L. Chen, and Y.-K. Chen, "High-speed low-voltage single-drove push-pull silicon Mach-Zehnder modulators," Opt. Express **19**, B26–B31 (2011).
22. Y. Yang, Q. Fang, M. Yu, X. Tu, R. Rusli, and G.-Q. Lo, "High-efficiency Si optical modulator using Cu travelling-wave electrode," Opt. Express **22**, 29978–29985 (2014).
23. D. Marris-Morini, L. Virot, C. Baudot, J.-M. Fédéli, D. Perez-Galacho, J.-M. Hartmann, S. Olivier, P. Brindel, P. Crozat, F. Boeuf, and L. Vivien, "A 40 Gbit/s optical link on a 300-mm silicon platform," Opt. Express **22**, 6674–6679 (2014).
24. L. Chen, C. R. Doerr, P. Dong, and Y.-K. Chen, "Monolithic silicon chip with 10 modulator channels at 25 Gbps and 100-GHz spacing," Opt. Express **19**, B946–B951 (2011).
25. H. Yu and W. Bogaerts, "An equivalent circuit model of the traveling wave electrode for carrier-depletion-based silicon optical modulators," J. Lightwave Technol. **30**, 1602–1609 (2012).
26. G. Ghione, *Semiconductor Devices for High-speed Optoelectronics* (Cambridge University, 2009), Chap. 6.
27. J. Lee, N. Kaneda, T. Pfau, A. Konczykowska, F. Jorge, J. Y. Dupuy, and Y. K. Chen, "Serial 103.125-Gb/s transmission over 1 km SSMF for low-cost, short-reach optical interconnects," in *Optical Fiber Communications Conference* (2014), paper Th2A.4.